

**DYNAMICAL BEHAVIOR AND  
MICROHETEROGENEITY OF  
CONFINED WATER IN QUATERNARY  
REVERSE MICELLES**

**NITIN YADAV**



**DEPARTMENT OF CHEMISTRY  
INDIAN INSTITUTE OF TECHNOLOGY DELHI  
AUGUST 2019**

**©Indian Institute of Technology Delhi (IITD), New Delhi, 2019**

# **DYNAMICAL BEHAVIOR AND MICROHETEROGENEITY OF CONFINED WATER IN QUATERNARY REVERSE MICELLES**

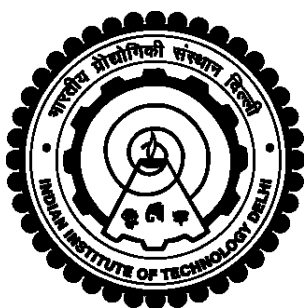
by

**Nitin Yadav**

**Department of Chemistry**

Submitted

in fulfillment of the requirements of the degree of Doctor of Philosophy  
to the



**INDIAN INSTITUTE OF TECHNOLOGY DELHI**

**AUGUST 2019**

*Dedicated to my Beloved Parents*

## CERTIFICATE

This is to certify that the thesis entitled, “**Dynamical Behavior and Microheterogeneity of Confined Water in Quaternary Reverse Micelles**”, being submitted by **Ms. Nitin Yadav** to the **Indian Institute of Technology Delhi** for the award of the degree of **Doctor of Philosophy** in Chemistry, is a record of bonafide research work carried out by her. **Miss Nitin Yadav** has worked under my guidance and supervision. She has fulfilled the requirements for the submission of this thesis, which to my knowledge has reached the requisite standard.

The results contained in this dissertation have not been submitted in part or full, to any other university or institute for award of any degree or diploma.

Date:

**Professor Pramit Kumar Chowdhury**  
Dept. of Chemistry  
Indian Institute of Technology Delhi  
New Delhi-110016  
INDIA

**Professor Ashok Kumar Ganguli**  
Dept. of Chemistry  
Indian Institute of Technology Delhi  
New Delhi-110016  
INDIA

## ACKNOWLEDGEMENTS

I would like to express my wholehearted gratitude to my research supervisor **Prof. Ashok Kumar Ganguli** and **Prof. Pramit Kumar Chowdhury** for their meticulous guidance, valuable suggestions, constructive criticism and constant encouragement throughout my Ph.D. tenure. Their untiring enthusiasm, immense support, scholarly inputs and help out of the way made me to conquer all the obstacles which I have experienced on this difficult path.

I would like to extend my sincerest thank to my research committee members, Prof. Siddharth Pandey, Prof. Shashank Deep and Prof. Bishwajit Kundu for their thoughtful comments and suggestions. I offer my thanks to all the past and the present Heads of the Department of Chemistry at IIT Delhi for providing me necessary facilities required for the completion of this thesis. I am also grateful to the DRC chairperson, all the faculty and staff members of the Department of Chemistry.

It is indeed my pleasure to express my thanks to my lab-colleagues; Dr. Menaka, Dr. Aparna Ganguly, Dr. Debashree Das, Dr. Sunita Khanchandani, Dr. Soma Sharma, Dr. Nibedita Das, Dr. Bharat, Dr. Gohil Thakur, Dr. Arabinda, Dr. Neha Garg, Dr. Kashinath, Dr. Zeba, Dr. Soumen Saha, Dr. Sandeep Kumar, Dr. Vaishali Sethi, Soumen Ash, Moumita Naskar, Preeti Dagar, Antara Sarkar, Dr. Anirban Das, Dr. Gajanan Kunde, Dr. Kalithasan, Shalini Tiwari, Priyanka Yadav, Kirandeep, Dr. Sanjib, Sandeep, Tripti and Harshita for their kind help and support.

Special thanks to my family; my father (Sh. B. S. Yadav), my mother (Smt. Geeta Yadav), my sister (Mamta Yadav) and my brother (Dipesh Yadav) for their unconditional support and love during this endeavor.

I highly acknowledge IIT Delhi for the financial support in PhD without which it would have been really difficult to carry out the research work.

Lastly, I would like to express my deepest thanks to Almighty God for giving me enough strength, patience and courage to complete my PhD.

Nitin Yadav

## ABSTRACT

This thesis entitled ‘**Dynamical Behavior and Microheterogeneity of Confined Water in Quaternary Reverse Micelles**’ focuses on understanding the molecular-level features of water pool in bare reverse micelles (RMs) and unveiling the in-detail intrinsic information of the temporal evolution of RMs *en route* nanorod formation and their underlying heterogeneity.

**Chapter 1** describes the background of RMs and their remarkable ability to tailor the structural characteristics of nanostructures. It also includes a brief overview on the dynamics and underlying heterogeneity of confined water in aqueous core of reverse micelles. **Chapter 2** describes the composition and synthesis of different nanostructures with the reverse micellar route along with the techniques used during the investigation. **Chapter 3** focuses on understanding the role of cosurfactant (1-butanol, 1-hexanol and 1-octanol) on the flexibility of interface of CTAB quaternary RMs by following the interfacial hydration dynamics using site-selective hydrophilic probe, Coumarin 343. The red edge excitation shift (REES) and dynamic Stokes shift measurements have been performed. The results showed the decrease in re-orientational mobility of water molecules with the increase in carbon chain length of cosurfactants. This infers the lower interfacial fluidity of CTAB RMs interface i.e. the more effective packing of RMs microstructure with 1-octanol as cosurfactant than that of RMs of butanol and RMs of hexanol. **Chapter 4** focuses on understanding the heterogeneous growth of anisotropic nanostructures in CTAB RMs by monitoring the local perturbations in different interior domains of assembly using site-selective solvation dynamics. The performed study proves that hydration dynamics can be a promising approach in tracking down the distinct growth periods of nanostructure evolution in RMs. In **Chapter 5**, we have made an attempt to unravel the role of interfacial flexibility via employing different cosurfactants, 1- butanol and 1-

octanol in giving rise to different morphology of nanostructures. The significantly retarded solvent response of RMs containing 1-octanol in comparison to that of RMs containing 1-butanol during the course of reaction is indicative of rigid micellar interface of former with respect to the latter. The obtained three distinct regions in the solvation profile during the evolution of both nanostructures, cubic-shaped and rod-shaped suggest a heterogeneous growth process. In **Chapter 6**, we have carried out a systematic study on the water-intake capacity of the microemulsion formed using a non-ionic surfactant, TX-100 with cosurfactants as 1-butanol and 1-hexanol. This RM system has been utilized for the synthesis of CdS nanoparticles. The effect of different concentrations of sodium salicylate (Na-Sal) on the nature of water molecules in the aqueous core of different sizes has been investigated using solvation dynamics of the C153 dye. In **Chapter 7**, we have summarized the major results of the performed studies in the present thesis and presented the future direction of this work.

# सार

यह थीसिस 'बेयर क्वाटरनरी रिवर्स माइकल्स के जलीय कोर के डायनामिकल पहलू और नैनोस्ट्रक्चर की वृद्धि के दौरान रिवर्स माइकल्स में पानी के पूल के आणविक स्तर की विशेषताओं को समझने और इन-डिटेल आंतरिक जानकारी का अनावरण करने पर केंद्रित है। रिवर्स माइकल्स के अस्थायी विकास एन मार्ग निर्माण और उनके अंतर्निहित विषमता को दर्शाता है।

अध्याय 1 में आरएम की पृष्ठभूमि और नैनोस्ट्रक्चर की संरचनात्मक विशेषताओं को दर्जी करने की उनकी उल्लेखनीय क्षमता का वर्णन है। इसमें डायनामिक्स पर एक संक्षिप्त अवलोकन और रिवर्स माइकल्स के जलीय कोर में सीमित पानी की विषमता भी शामिल है। अध्याय 2 में जांच के दौरान उपयोग की जाने वाली तकनीकों के साथ रिवर्स माइक्रेलर मार्ग के साथ विभिन्न नैनोस्ट्रक्चर की संरचना और संश्लेषण का वर्णन किया गया है। अध्याय 3 साइट-चयनात्मक हाइड्रोफिलिक जांच, कामारिन 343 का उपयोग करके इंटरसैशनल हाइड्रेशन डायनामिक्स का अनुसरण करके CTAB चतुष्कोणीय आरएम के इंटरफ़ेस के लचीलेपन पर कॉसर्फैक्टेंट (1-ब्यूटेनॉल, 1-हेक्सानॉल और 1-ऑक्टानॉल) की भूमिका को समझने पर केंद्रित है। उत्तेजना बदलाव (REES) और गतिशील स्टोक्स शिफ्ट माप प्रदर्शन किया गया है। परिणामों ने कॉर्फुरैक्टेंट्स की कार्बन श्रृंखला लंबाई में वृद्धि के साथ पानी के अणुओं की पुनः ओरिएंटेशनल गतिशीलता में कमी को दिखाया। यह CTAB RMs इंटरफ़ेस की कम इंटरफेशियल फ्लुइडिटी को

प्रभावित करता है यानी 1-ऑक्टैनाॅल के साथ RMS माइक्रोस्ट्रक्चर की अधिक प्रभावी पैकिंग कॉसुरल के रूप में ब्यूटेनाॅल और हेमैनाॅल के RMs की तुलना में अधिक है। अध्याय 4 साइट-चयनात्मक सॉल्वेशन डायनेमिक्स का उपयोग करके विधानसभा के विभिन्न आंतरिक डोमेन में स्थानीय गड़बड़ियों की निगरानी करके CTAB RMs में अनीसोट्रोपिक नैनोस्ट्रक्चर के विषम विकास को समझने पर केंद्रित है। प्रस्तुत अध्ययन यह साबित करता है कि आरएम में नैनोस्ट्रक्चर विकास के विभिन्न विकास अवधियों को ट्रैक करने में जलयोजन गतिशीलता एक आशाजनक दृष्टिकोण हो सकता है। अध्याय 5 में, हमने विभिन्न कॉसुरफैक्टेंट्स, 1- ब्यूटेनाॅल और 1- ऑक्टैनाॅल को नैनोस्ट्रक्चर के विभिन्न आकारिकी को जन्म देने के माध्यम से इंटरफेसियल लचीलेपन की भूमिका को उजागर करने का प्रयास किया है। आरएम की तुलना में 1-ऑक्टैनाॅल युक्त आरएमएस की तुलना में 1-ब्यूटेनाॅल युक्त काफी मंद विलायक प्रतिक्रिया, उत्तरार्द्ध के संबंध में पूर्व के कठोर माइक्रेलर इंटरफेस का संकेत है। दोनों नैनोस्ट्रक्चर, क्यूबिक-शेप और रॉड-शेप के विकास के दौरान सॉल्वेशन प्रोफाइल में तीन अलग-अलग क्षेत्र एक विषम विकास प्रक्रिया का सुझाव देते हैं। अध्याय 6 में, हमने 1-ब्यूटेनाॅल और 1-हेक्सांनाॅल के रूप में कोर्फैक्ट के साथ गैर-आयनिक सर्फैक्टेंट, TX-100 का उपयोग करके गठित माइक्रोएल्शन की जल-सेवन क्षमता पर एक व्यवस्थित अध्ययन किया है। इस RM प्रणाली का उपयोग CdS नैनोकणों के संश्लेषण के लिए किया गया है। विभिन्न आकारों के जलीय मूल में पानी के

अणुओं की प्रकृति पर सोडियम सैलिसिलेट (Na-SaI) के विभिन्न सांद्रता के प्रभाव की जांच C153 डाई की सॉल्वेंस गतिशीलता का उपयोग करके की गई है। अध्याय 7 में, हमने वर्तमान थीसिस में किए गए अध्ययन के प्रमुख परिणामों को संक्षेप में प्रस्तुत किया है और इस कार्य की भविष्य की दिशा प्रस्तुत की है।

## TABLE OF CONTENTS

CERTIFICATE		i
ACKNOWLEDGEMENTS		ii
ABSTRACT		iv
संर		vi
TABLE OF CONTENTS		ix
LIST OF FIGURES		xiii
LIST OF TABLES		xix
ABBREVIATIONS AND SYMBOLS		xxi
Chapter 1	<b>Introduction</b>	1–43
1.1	Introduction	2
1.2	Microemulsions	3
1.2.1	Surfactants	5
1.2.2	Cosurfactants	8
1.3	Reverse Micelles	9
1.3.1	Ternary Systems	9
1.3.2	Quaternary Systems	10
1.4	Characterization of Reverse Micelles	11
1.4.1	Methods demonstrating the presence of Reverse Micelles (RMs)	11
1.5	Synthesis of Nanoparticles in Reverse Micelles	13
1.6	Dynamics of Reverse Micelles	16
1.7	Solvation Dynamics	17
1.7.1	Basic Features of Solvation Dynamics	19
1.8	Dynamics of Water Confined to Microheterogeneous System of Reverse Micelles	23
1.9	Thesis Outline	25
1.10	References	28

Chapter 2	<b>Materials and Methods</b>	44–70
2.1	Materials and Methods	45
2.1.1	Materials	45
2.1.2	Sample Preparation	45
2.2	Spectroscopic Methods	47
2.2.1	UV-Vis Absorption spectroscopy	47
2.2.2	Fluorescence spectroscopy	48
2.2.2.1	Steady State Fluorescence Measurements	51
2.2.3	Time Resolved Fluorescence Spectroscopy	51
2.2.3.1	Time Correlated Single Photon Counting technique (TCSPC)	54
2.2.3.2	Basic Principle of TCSPC Technique	55
2.2.3.3	Data Analysis	58
2.2.4	Time-Resolved Emission Spectra (TRES)	60
2.2.5	Solvent Correlation Function	62
2.2.6	Time-resolved Fluorescence Anisotropy	64
2.3	References	67
Chapter 3	<b>Understanding the Interfacial flexibility in CTAB based reverse micellar droplets using solvation dynamics: Role of cosurfactant</b>	71–93
3.1	Introduction	73
3.2	Results	75
3.2.1	Red Edge Excitation Shift Study (REES)	75
3.2.2	Dynamic Fluorescence Stokes Shift Measurements	76
3.3	Discussion	79
3.4	Conclusions	89
3.5	References	89

Chapter 4	<b>Mechanistic Insights on the Growth of Anisotropic Nanostructures inside Reverse Micelles: A Solvation Perspective</b>	94–142
4.1	Introduction	96
4.2	Results	98
4.3	Discussion	123
4.4	Conclusions	136
4.5	References	136
Chapter 5	<b>Role of interfacial flexibility in controlling the different morphologies of anisotropic copper oxalate nanostructures in CTAB Reverse micelles: Role of cosurfactant</b>	143–171
5.1	Introduction	145
5.2	Results	146
5.3	Discussion	158
5.4	Conclusions	167
5.5	References	167
Chapter 6	<b>Understanding the microenvironment of confined nanopools in new quaternary reverse micelle system based on TX-100 (neutral surfactant) using solvation dynamics</b>	172–190
6.1	Introduction	174
6.2	Results	175
6.2.1	Study of the water-intake capacity of RMs (TX-100/isooctane/cosurfactant (butanol/hexanol)/water)	175
6.2.2	Synthesis of CdS nanoparticles	175
6.2.3	Fluorescence Measurements	178
6.2.3.1	Steady state fluorescence studies	178

6.2.3.2	Dynamic Fluorescence Stokes shift studies	180
6.3	Discussion	181
6.4	Conclusions	187
6.5	References	187
Chapter 7	Conclusions and Future Prospects	191–195
Biodata		196

## List of Figures

Figure No.	Figure Captions	Page No.
1.1	Phase diagram of a polar and nonpolar phase with a surfactant showing the area of stability of w/o- and o/w-microemulsions	4
1.2	Schematic representation of the various self-assembled supramolecular aggregate structures of the surfactant molecules	7
1.3	Schematic presentation of water-in-oil microemulsion droplets (reverse micelles)	11
1.4	Strategies for ME-based nanoparticle synthesis: a) Two MEs containing individual reactant (A and B); b) ME with one reactant (A) and addition of an aqueous solution of other reactant (B); c) ME containing both the reactant (A+B) and external initiation (e.g. pH and temperature); d) ME having one reactant (A) in the polar droplet phase and the other reactant (B) is present in the apolar dispersant phase	15
1.5	Schematic depiction of the mechanism of the formation of nanoparticles in RMs via fused dimer formed after the coalescence of two MEDs which gave rise to the nanochannels in between.	16
1.6	Schematic presentation of solvation of an ion (or dipole by water). The solute-solvent system is in minimum energy configuration	19
1.7	Schematic illustration of the potential energy surfaces involved in solvation dynamics showing the water orientational motions along the solvation coordinate together with instantaneous polarization P	21
1.8	Some solvatochromic probes which are commonly used for the Solvation dynamics experiments (A) Coumarin 343 (C343) (B) Coumarin 153 (C153) (C) Coumarin 480 (C480) (D) <i>N,N</i> -Dimethyl-6-propionyl-2-naphthylamine (Prodan)	22
2.1	The Jablonski diagram represents the various processes followed by the light absorption	49
2.2	A Schematic depiction of time domain fluorescence lifetime measurements	54
2.3	Principle of TCSPC technique	56
2.4	A conventional TCSPC arrangement	56

2.5	Solvation dynamics: (A) Decrease in the energy of the excited state; (B) Wavelength-dependent fluorescence decays; (C) Time-resolved emission spectra	63
2.6	Schematic presentation of the measurement of the fluorescence anisotropies	65
3.1	[I] Emission spectra at various excitation wavelengths ( $\lambda_{ex}$ ) and [II] TRES (Time resolved emission) plots of probe C343 in CTAB RMs of different cosurfactants, butanol (A), hexanol (B) and Octanol (C) at $W_o$ value of 4	77
3.2	[I] Emission spectra at various excitation wavelengths ( $\lambda_{ex}$ ) and [II] TRES plots of probe C343 in CTAB RMs of different cosurfactants, butanol (A), hexanol (B) and Octanol (C) at $W_o$ value of 8	78
3.3	[I] Emission spectra at various excitation wavelengths ( $\lambda_{ex}$ ) and [II] Time resolved emission spectra at different times of probe C343 in CTAB RMs of different cosurfactants, butanol (A), hexanol (B) and Octanol (C) at $W_o$ value of 12	79
3.4	[I] Emission spectra at various excitation wavelengths ( $\lambda_{ex}$ ) and [II] Time resolved emission spectra at different times of probe C343 in CTAB RMs of different cosurfactants, butanol (A), hexanol (B) and Octanol (C) at $W_o$ value of 16	80
3.5	[I] Emission spectra at various excitation wavelengths ( $\lambda_{ex}$ ) and [II] Time resolved emission spectra at different times of probe C343 in CTAB RMs of different cosurfactants, butanol (A), hexanol (B) and Octanol (C) at $W_o$ value of 20	81
3.6	[I] Emission spectra at various excitation wavelengths ( $\lambda_{ex}$ ) and [II] Time resolved emission spectra at different times of probe C343 in CTAB RMs of different cosurfactants, butanol (A), hexanol (B) and Octanol (C) at $W_o$ value of 24	82
3.7	[I] Emission spectra at various excitation wavelengths ( $\lambda_{ex}$ ) and [II] Time resolved emission spectra at different times of probe C343 in CTAB RMs of different cosurfactants, butanol (A), hexanol (B) and Octanol (C) at $W_o$ value of 30	83
3.8	[I] Emission spectra at various excitation wavelengths ( $\lambda_{ex}$ ) and [II] Time resolved emission spectra at different times of probe C343 in CTAB RMs of different cosurfactants, butanol (A), hexanol (B) and Octanol (C) at $W_o$ value of 40	84
3.9	A plot of the REES shift of C343 in the CTAB RMs as a function of the increasing carbon chain length of cosurfactants (butanol, hexanol and octanol) at various $W_o$ values of 4, 8, 12, 16, 20, 24, 30 and 40	85

3.10	A plot of the REES shift of C343 in the CTAB RMs as a function of the increasing $Wo$ values (4, 8, 12, 16, 20, 24, 30 and 40) for different cosurfactants (butanol, hexanol, octanol)	85
3.11	Decay of solvent response function, $C(t)$ , of C343 in CTAB RMs of different cosurfactants, butanol, hexanol and octanol at different $Wo$ values of 4 (A), 8 (B), 12 (C), 16 (D), 20 (E), 24 (F), 30 (G) and 40 (H)	86
3.12	A plot of the $\langle\tau_s\rangle$ of C343 in CTAB RMs as a function of the increasing carbon chain length of the cosurfactants (butanol, hexanol and octanol) at various $Wo$ values of 4, 8, 12, 16, 20, 24, 30 and 40	88
3.13	A plot of the $\langle\tau_s\rangle$ of C343 in CTAB RMs as a function of the increasing $Wo$ values for cosurfactants, butanol, hexanol and octanol	88
4.1	Emission spectra of the solvation probes C343 and C153 in Iron oxalate (FeOx) RM system. [A] Emission spectra of C343 in pure RMs ( $H_2O$ ), RMs containing reactants (AmOx and FeNt) and RMs having FeOx nanostructures; [B] Emission spectra of C343 in pure RMs ( $H_2O$ ), RMs containing reactants (AmOx and FeNt) and RMs after extracting the FeOx nanostructures; [C] Emission spectra of C153 in pure RMs ( $H_2O$ ), RMs containing reactants (AmOx and FeNt) and RMs having FeOx nanostructures; [D] Emission spectra of C153 in pure RMs ( $H_2O$ ), RMs containing reactants (AmOx and FeNt) and RMs after extracting the FeOx nanostructures	99
4.2	Emission spectra of solvation probes C343 and C153 in Zinc oxalate reverse RMs system. [A] Emission spectra of C343 in pure RMs ( $H_2O$ ), RMs containing reactants (AmOx and ZnNt) and RMs having ZnOx nanostructures; [B] Emission spectra of C343 in pure RMs ( $H_2O$ ), RMs containing reactants (AmOx and ZnNt) and RMs after extracting the ZnOx nanostructures; [C] Emission spectra of C153 in pure RMs ( $H_2O$ ), RMs containing reactants (AmOx and ZnNt) and RMs having ZnOx nanostructures; [D] Emission spectra of C153 in pure RMs ( $H_2O$ ), RMs containing reactants (AmOx and ZnNt) and RMs after extracting the ZnOx nanostructures	100
4.3	Representative TRES plots of C343 in RMs encapsulating FeOx nanostructures at different time intervals of synthesis (A: Day 0; B: Day 2; C: Day 3; D: Day 4; E: Day 5)	103
4.4	Representative TRES plots of C343 in surfactant aggregates in supernatant solution after extracting FeOx nanostructures at different time intervals of synthesis (A: Day 0; B: Day 2; C: Day 3; D: Day 4; E: Day 8)	103

4.5	Representative TRES plots of C153 in RMs encapsulating FeOx nanostructures at different time intervals of synthesis (A: Day 0; B: Day 2; C: Day 4; D: Day 8)	104
4.6	Representative TRES plots of C153 in surfactant aggregates in supernatant solution after extracting FeOx nanostructures at different time intervals of synthesis (A: Day 0; B: Day 2; C: Day 4; D: Day 8)	104
4.7	Representative TRES plots of C343 in surfactant aggregates in supernatant solution after extracting ZnOx nanostructures at different time intervals of synthesis (A: 0 hr; B: 3 <sup>th</sup> hr; C: 6 <sup>th</sup> hr; D: 9 <sup>th</sup> day; E: 15 <sup>th</sup> hr)	105
4.8	Representative TRES plots of C153 in surfactant aggregates in supernatant solution after extracting ZnOx nanostructures at different time intervals of synthesis (A: 0 hr; B: 2 <sup>nd</sup> hr ; C: 3 <sup>rd</sup> hr; D: 4 <sup>th</sup> hr; E: 10 <sup>th</sup> hr; F: 15 <sup>th</sup> hr)	105
4.9	Decay of solvent response function, $C(t)$ , of C343, [A] in pure RMs, reactant (AmOx and FeNt) containing RMs and RMs encapsulating FeOx nanostructures, [B] in pure RMs, reactant (AmOx and FeNt) containing RMs and in surfactant aggregates obtained after extracting evolved FeOx nanostructures	106
4.10	Decay of solvent response function, $C(t)$ , of C153, [A] in pure RMs, reactant (AmOx and FeNt) containing RMs and RMs encapsulating FeOx nanostructures, [B] in pure RMs, reactant (AmOx and FeNt) containing RMs and in surfactant aggregates obtained after extracting evolved FeOx nanostructures	106
4.11	Decays of solvent correlation function, $C(t)$ , of C343 (A) and C153 (B) in Pure (H <sub>2</sub> O) RMs, reactant (AmOx and ZnNt) containing reverse micelles and in micellar aggregates in supernatant solution after extracting ZnOx nanostructures	107
4.12	Plot of the average solvation time, ( $\langle\tau\rangle$ ) and the slowest solvation time, ( $\tau_s$ ) as a function of increasing reaction time (day) in reverse micelles encapsulating FeOx nanostructures and in surfactant aggregated structures in supernatant solution obtained after extracting evolved FeOx nanostructures during the synthesis	110
4.13	Plot of the average solvation time, ( $\tau$ ) of C343 (A) and C153 (B) as a function of increasing reaction time (hr) in surfactant aggregated structures in supernatant solution obtained after extracting the ZnOx nanostructures during synthesis	116
4.14	Schematic representation of the proposed stages in the growth of anisotropic FeOx nanostructures inside the aqueous core of RMs	129

5.1	TEM Micrographs of CuOx rod-shaped and cube-shaped nanostructures synthesized using CTAB/1-butanol/isooctane/H <sub>2</sub> O and CTAB/1-octanol/isooctane/H <sub>2</sub> O RM system respectively	147
5.2	Emission spectra of C343 probe inside the CTAB/1-butanol/isooctane/H <sub>2</sub> O (I) and CTAB/1-octanol/isooctane/H <sub>2</sub> O (II) RMs. [A: pure RMs (H <sub>2</sub> O), RMs containing reactants (AmOx and CuNt) and RMs encapsulating CuOx nanostructures; B: pure RMs (H <sub>2</sub> O), RMs containing reactants (AmOx and CuNt) and surfactant aggregates present in supernatant solution (obtained after the extraction of CuOx nanoparticles from the core of RMs)]	149
5.3	Normalized TRES plots of C343 inside the CTAB/1-butanol/isooctane/H <sub>2</sub> O (I) and CTAB/1-octanol/isooctane/H <sub>2</sub> O (II) RMs. [A: pure RMs; B: AmOx-containing RMs; C: CuNt-containing RMs	150
5.4	Normalized TRES plots of C343 in surfactant aggregates present in supernatant solution which obtained after the extraction of CuOx nanoparticles from CTAB/1-butanol/isooctane/H <sub>2</sub> O RMs. (A: 0 hr; B: 1 hr; C: 2 hr; D: 3hr; E: 4 hr; F: 5 hr; G: 6 hr; H: 7 hr)	151
5.5	Normalized TRES plots of C343 in surfactant aggregates present in supernatant solution which obtained after the extraction of CuOx nanoparticles from CTAB/1-butanol/isooctane/H <sub>2</sub> O RMs. (A: 8 hr; B: 9 hr; C: 10 hr; D: 11 hr; E: 12 hr; F: 13 hr; G: 14 hr; H: 15 hr)	152
5.6	Normalized TRES plots of C343 in surfactant aggregates present in supernatant solution which obtained after the extraction of CuOx nanoparticles from CTAB/1-octanol/isooctane/H <sub>2</sub> O RMs. (A: 0 hr; B: 1 hr; C: 2 hr; D: 3 hr; E: 4 hr; F: 5 hr; G: 6 hr; H: 7 hr)	153
5.7	Normalized TRES plots of C343 in surfactant aggregates present in supernatant solution which obtained after the extraction of CuOx nanoparticles from CTAB/1-octanol/isooctane/H <sub>2</sub> O RMs. (A: 8 hr; B: 9 hr; C: 10 hr; D: 11 hr; E: 12 hr; F: 13 hr; G: 14 hr; H: 15 hr)	154
5.8	Representative decays of solvent correlation function, C(t) of C343 in pure RMs (H <sub>2</sub> O), in reactant-containing RMs and in surfactant aggregates present in supernatant solution obtained after the extraction of CuOx nanoparticles (A: CTAB/1-butanol/isooctane/H <sub>2</sub> O RM system; B: CTAB/1-octanol/isooctane/H <sub>2</sub> O RM system)	155

5.9	Plot of the slowest solvation time, ( $\tau_{s2}$ ) and average solvation time, ( $\tau_s$ ) as a function of increasing reaction time (hr) in bare surfactant aggregated structures in supernatant solution obtained after the extraction of CuOx nanostructures (CTAB/1-butanol/isooctane/H <sub>2</sub> O RM system; CTAB/1-octanol/isooctane/H <sub>2</sub> O RM system)	155
6.1	Water-intake capacity for TX-100/1-hexanol/isooctane/water system on a pseudoternary phase diagram (the regions have been shaded for better clarity)	176
6.2	Water-intake capacity for TX-100/1-butanol/isooctane/water system on a pseudoternary phase diagram (the regions have been shaded for better clarity)	176
6.3	Powder X-ray diffraction pattern of CdS nanoparticles synthesized using TX-100/1-butanol/isooctane/H <sub>2</sub> O RM system	177
6.4	TEM Micrograph of CdS nanoparticles synthesized using TX-100/1-butanol/isooctane/H <sub>2</sub> O RM system	178
6.5	Steady-state emission spectra of C153 in TX-100 RMs for Wo values of 2, 12, 30 at different R values	179
6.6	Steady-state emission spectra of C153 in TX-100 RMs at Ro values of 0, 0.2, 0.6 and 1 for different Wo values	181
6.7	TRES plots of C153 in TX-100 RMs at different values of R for Wo2	182
6.8	TRES plots of C153 in TX-100 RMs at different values of R for Wo12	182
6.9	TRES plots of C153 in TX-100 RMs at different values of Ro for Wo 30	183
6.10	Decay of solvent response function, C(t) of C153 in TX-100 RMs at different values of Ro for Wo value of 2, 12 and 30	

## List of Tables

Table No.	Table Tittle	Page No.
1.1	Categorization of the surfactants depending on the charge	5
1.2	Different expected micellar structural aggregates based on critical packing parameter	7
3.1	Decay parameters of solvent correlation function, $C(t)$ , of C343 in RMs of different cosurfactants as butanol, hexanol and octanol at $W_o$ values of 4, 8, 12, 16, 20, 24, 30, 40	87
4.1	Decay parameters of solvent correlation function, $C(t)$ , of C343 during the synthesis of the FeOx nanostructures	108
4.2	Decay parameters of solvent correlation function, $C(t)$ , of C343 in Pure RMs, in (AmOx and FeNt) reactant-containing RMs and surfactant aggregates in supernatant solution after extracting FeOx Nanostructures (over eight consecutive days)	109
4.3	Decay parameters of solvent correlation function, $C(t)$ , of C153 during the synthesis of the FeOx nanostructures	111
4.4	Decay parameters of solvent correlation function, $C(t)$ , of C153 in Pure RMs, in AmOx and FeNt as reactant-containing RMs and surfactant aggregates in supernatant solution obtained after extracting FeOx Nanostructures (over eight consecutive days)	112
4.5	Decay parameters of the solvent correlation function, $C(t)$ , of C343 in Pure RMs, in AmOx and ZnNt as reactant-containing RMs and CTAB-aggregated structures in supernatant solution obtained after extracting ZnOx Nanostructures over a period of 15 hrs	114
4.6	Decay parameters of the solvent correlation function, $C(t)$ , of C153 in Pure RMs, in AmOx and ZnNt as reactant-containing RMs and CTAB-aggregated structures in supernatant solution after extracting ZnOx Nanostructures over a period of 15 hrs	115
4.7	Anisotropy decay parameters of C343 during the synthesis of the FeOx nanostructures	117
4.8	Anisotropy decay parameters of C343 in Pure RMs, in RMs containing reactants (AmOx and FeNt) and surfactant aggregates in supernatant solution after extracting FeOx nanostructures (over eight consecutive days)	118
4.9	Anisotropy decay characteristics of C153 during the synthesis of the FeOx nanostructures	119

4.10	Anisotropy decay parameters of C153 in Pure RMs, in RMs containing reactants (AmOx and FeNt) and surfactant aggregates in supernatant solution after extracting FeOx nanostructures (over eight consecutive days)	120
4.11	Anisotropy decay parameters of C343 in Pure RMs, in RMs containing reactants (AmOx and ZnOx) and aggregated structures in supernatant solution after extracting ZnOx nanostructures over consecutive 15 hr	121
4.12	Anisotropy decay parameters of C153 in Pure RMs, in RMs containing reactants (AmOx and ZnOx) and aggregated structures in supernatant solution after extracting ZnOx nanostructures over consecutive 15 hr	122
5.1	Decay Parameters of Solvent Correlation function, $C(t)$ , of C343 in CTAB/1-butanol/isooctane/H <sub>2</sub> O RMs, RMs containing reactants (AmOx and CuNt) and bare CTAB-aggregated structures in supernatant solution obtained after the extraction of CuOx nanostructures over consecutive 15 hr (duration of reaction)	156
5.2	Decay Parameters of Solvent Correlation function, $C(t)$ , of C343 in CTAB/1-octanol/isooctane/H <sub>2</sub> O RMs, RMs containing reactants (AmOx and CuNt) and bare CTAB-aggregated structures in supernatant solution obtained after the extraction of CuOx nanostructures over consecutive 15 hr (duration of reaction)	157
5.3	Anisotropy decay characteristics of C343 in CTAB/1-butanol/isooctane/H <sub>2</sub> O RMs, RMs containing reactants (AmOx and CuNt) and bare CTAB-aggregated structures in supernatant solution obtained after the extraction of CuOx nanostructures over consecutive 15 hr (duration of reaction)	159
5.4	Anisotropy decay characteristics of C343 in CTAB/1-octanol/isooctane/H <sub>2</sub> O RMs, RMs containing reactants (AmOx and CuNt) and bare CTAB-aggregated structures in supernatant solution obtained after the extraction of CuOx nanostructures over consecutive 15 hr (duration of reaction)	160
6.1	Decay parameters of Solvent Correlation Function, $C(t)$ of C153 in TX-100 RMs at $W_o$ values of 2, 12 and 30 for different values of $Ro$	184

## Abbreviations and Symbols

nm	nanometer
h	hour
$\lambda$	wavelength
RM	reverse micelles
ME	microemulsion
MEDs	microemulsion droplets
Wo	[Water]/[Surfactant]
TEM	transmission Electron Microscopy
UV-Vis	ultra violet visible spectroscopy
REES	red edge excitation shift
TRES	time resolved emission spectra
ns	nanosecond
ps	picosecond